HAL
open science

Reconstruction of the rose of directions from a digital micro-hologram of fibers

Loïc Denis, Thierry Fournel, Corinne Fournier, Dominique Jeulin

To cite this version:

Loïc Denis, Thierry Fournel, Corinne Fournier, Dominique Jeulin. Reconstruction of the rose of directions from a digital micro-hologram of fibers. Journal of Microscopy, 2007, 225 (3), pp.283-292. 10.1111/j.1365-2818.2007.01744.x . ujm-00116998v2

HAL Id: ujm-00116998
https://ujm.hal.science/ujm-00116998v2

Submitted on 3 Jun 2008

HAL is a multi-disciplinary open access archive for the deposit and dissemination of scientific research documents, whether they are published or not. The documents may come from teaching and research institutions in France or abroad, or from public or private research centers.

L'archive ouverte pluridisciplinaire **HAL**, est destinée au dépôt et à la diffusion de documents scientifiques de niveau recherche, publiés ou non, émanant des établissements d'enseignement et de recherche français ou étrangers, des laboratoires publics ou privés.

Copyright notice

This paper was published in Journal of Microscopy, a Blackwell Publishing Journal published on behalf of the Royal Microscopical Society. It is made available as an electronic reprint with the permission of Blackwell Publishing. The reference of the article is :
"Reconstruction of the rose of directions from a digital microhologram of fibres", Loïc Denis, Thierry Fournel, Corinne Fournier & Dominique Jeulin, Journal of Microscopy, Volume 225, Issue 3, Page 283-292, Mar 2007.
(doi : `10.1111/j.1365-2818.2007.01744.x`).
The definitive version is available at `www.blackwell-synergy.com`.

Reconstruction of the rose of directions from a digital micro-hologram of fibers

Loïc Denis, Thierry Fournel, Corinne Fournier

Laboratoire Traitement du Signal et Instrumentation

UMR CNRS 5516

Bât. F, 10 rue Barrouin, 42000 Saint-Etienne, France

loic.denis@univ-st-etienne.fr

Dominique Jeulin

Centre de Morphologie Mathématique

Ecole des Mines de Paris

35 rue Saint-Honoré, 77300 Fontainebleau, France

Digital holography makes it possible to acquire quickly the interference patterns of objects spread in a volume. The digital processing of the fringes is still too slow to achieve on line analysis of the holograms. We describe a new approach to obtain information on the direction of illuminated objects. The key idea is to avoid reconstruction of the volume followed by classical three-dimensional image processing. The hologram is processed using a global analysis based on autocorrelation. A fundamental property of diffraction patterns leads to an estimate of the mean geometric-covariogram (MGC) of the objects projections. The rose of directions is connected with the MGC through an inverse problem. In the general case, only the 2D rose of the object projections can be reconstructed. The further assumption of unique-size objects gives access with the knowledge of this size to the 3D direction information. An iterative scheme is suggested to reconstruct the 3D rose in this special case. Results are provided on holograms of paper fibers.

1. Introduction

Non-intrusive on-line control is of great importance in most production processes. In the case of 3D moving objects, designing this control is challenging. To track the directions of small objects spread in a volume one requires both a fast 3D imaging facility and an efficient image processing scheme.

Holography is a technique that allows a description of a three-dimensional distribution of objects to be stored on a two-dimensional detector. It ensures non intrusive control of still or moving objects. The recording of the hologram on a digital camera suppresses the wet chemical processing step and makes it possible to acquire and analyze volume objects within a short time, the limiting factor being the numerical processing speed. It gives rise to a whole range of potential algorithms for the processing of the holograms. Digital holography has been widely studied these last years (see recent contributions published in (Poon *et al.*, 2006)) and applied to many different fields such as microscopy, particle image velocimetry and deformation analysis. It plays an important role for the study of small objects and is used in fluid mechanics for 3D flow visualization.

Since fast acquisition of 3D objects is possible with digital holography, we focus in this article on the hologram processing. We describe a method to study the direction of fibers randomly distributed in a volume from a single hologram. We follow an original stereological approach that differs from classical analysis of the volume reconstructed from the hologram. This work follows a sizing method based on the hologram-autocorrelation analysis (Denis *et al.*, 2006).

To quantify anisotropy of the fiber distribution, a statistical representation is often used: the rose of directions R (Serra, 1982). It is the distribution of directions weightened by the mean fiber-length in each direction. If the fiber process is isotropic, then R is the uniform distribution. By contrast, the fact that R is uniform does not imply that the underlying fiber process is isotropic (Serra, 1982; Stoyan & Beneš, 1991; Kiderlen & Pfrang, 2005). A non-uniform rose of directions clearly indicates anisotropy. In particular, preferred directions of a fiber system can be detected (Kiderlen & Pfrang, 2005). The estimation of R requires

either direct measurement of spatial directions or an indirect approach. In the latter case, R is derived from another quantity carrying the same directional information while being directly estimated from the data. The mean geometric covariogram (MGC) (Serra, 1982), defined as the autocorrelation of an object, averaged over the objects population, is such a quantity. Another commonly used quantity to derive R is the rose of intercepts γ, defined as the diametral variation in a given direction (Serra, 1982).

After a short introduction to digital holography (section 2), we derive the rose of directions of the fibers projections from their mean geometric covariogram computed from the hologram. The mean geometric covariogram of the objects projections is estimated directly from the hologram (section 3). In the general case, only the 2D rose of directions can be derived from the estimated MGC (section 4). With a further assumption one can reconstruct the 3D rose of the objects. An iterative reconstruction algorithm is suggested in this case and the method is illustrated on simulated and experimental holograms (section 5).

2. In-line digital holography

Let's give a preliminary description of in-line digital holography to introduce the basics and the notations we will follow in the next sections.

The in-line holography recording setup, also named "Gabor holography" after its inventor, involves no imaging lens. The intensity of the incident coherent beam, diffracted when crossing the objects and free propagated beyond is recorded on the sensor (a digital camera) (see Figure 1). This setup, used to record holograms of small opaque objects such as microparticles or fibers, is robust with respect to vibrations thanks to the unique beam used. Increasing the concentration of objects yields a degradation of the hologram quality due to speckle noise. This technique therefore is restricted to collections of objects whose projected surface on the hologram plane remains under a limit (1% of the hologram surface) (Royer, 1974).

The recorded hologram can be explained as the interference pattern between two beams: the reference beam and the objects beam. Unlike with two-beams setups, in Gabor holog-

raphy there is a single beam which can be interpreted past the objects as the superposition of two waves: a reference wave identical to the incident wave and a object wave emerging from the objects (Goodman, 1996). In all-optic holography, the reconstruction is led by re-illuminating the hologram with the reference beam. The hologram then diffracts the beam and gives rise to the real and virtual images. Diffraction of a plane wave by a plane object of given transmittance t can be modeled under Fresnel approximation as a spatial convolution (Goodman, 1996). The complex amplitude $\underline{A_z}$ of the diffracted wave in a plane located at a distance z related to the objects is given by:

$$\underline{A_z}(x,y) = \left(t * \underline{h_z}\right)(x,y) \tag{1}$$

with the following kernel:

$$\underline{h_z}(x,y) = 1/(i\lambda z)\exp\left[i\pi(x^2+y^2)/(\lambda z)\right]$$

where i stands for the imaginary unit, λ is the wavelength and $*$ denotes the two-dimensional convolution. The complex amplitude $\underline{A_z}$ is called the Fresnel transform of transmittance function $\underline{t}$ with parameter λz (scale parameter). Since diffraction governs both the hologram formation and its reconstruction, Fresnel transform is a fundamental tool for both hologram modeling and digital reconstruction.

Fresnel transform is a totally redundant scaling transform (Onural, 1993). By changing the scale parameter, images can be reconstructed at various depths z. The redundancy of the transform results in the presence of out-of-focus objects in the reconstructed images. These out-of-focus objects appear as low contrast concentric fringes. The numerical transform is performed using Fast Fourier transforms and a digital focusing is obtained by modifying the parameter z of the convolution kernel.

3. Estimating the mean geometric covariogram of the objects projections

We derive in this section an estimate of the mean geometric covariogram (MGC) of the objects projections from the expression of the hologram intensity.

In the context of in-line holography of small opaque objects, the hologram intensity is related with the objects through a diffraction phenomenon. If we consider the incoming wave to remain quasi-plane for each object, which is justified for holograms of low-concentration collections of objects, the resulting diffracted wave in the recording plane is (Denis *et al.*, 2006):

$$\underline{A} \approx 1 - \sum_{j=1}^{N} \vartheta_j * \underline{h_{z_j}} * \delta_{x_j,y_j}$$

where z_j is the distance between object j and the recording plane, N is the number of objects, ϑ_j denotes the aperture of object j, δ_{x_j,y_j} stands for Dirac's distribution centered in (x_j, y_j). In this expression, the first term can be interpreted as the reference wave (with normalized energy and null phase in the hologram plane) ; the other term is a sum of the contribution of each object. These contributions are complex valued and are summed up.

The recorded signal in the hologram plane corresponds to the intensity I_H of the wave, related to the complex amplitude via the following relation: $I_H = |\underline{A_{z_r}}|^2$. The hologram intensity can therefore be expanded as follows:

$$I_H = 1 - 2\sum_{j=1}^{N} \vartheta_j * \Re(\underline{h_{z_j}}) * \delta_{x_j,y_j} + \sum_{j=1}^{N}\sum_{k=1}^{N} \left(\vartheta_j * \underline{h_{z_j}} * \delta_{x_j,y_j}\right) \times \left(\vartheta_k * \underline{h_{-z_k}} * \delta_{x_k,y_k}\right), \quad (2)$$

where $\Re$ denotes the real part of a complex number. The first term is constant and corresponds to the reference wave, the second term is the sum of all diffraction patterns, and the last term expresses both inter-object interferences ($j \neq k$) and the non-linear component of a diffraction pattern ($j = k$) . Under the hypothesis of both small objects and low-concentration holograms, the third term can be neglected. This gives the following linear hologram-formation approximation:

$$I_H \approx 1 - 2\sum_{j=1}^{N} \vartheta_j * \Re(\underline{h_{z_j}}) * \delta_{x_j,y_j}. \quad (3)$$

When considering objects with a random distribution in space, implanted on points of a 3D homogeneous Poisson point process with intensity c (i.e. c is the average number of points per unit volume), the hologram can then be described in the context of random set models as a dilution random function (Serra, 1968; Jeulin, 1992). The primary functions $\vartheta_j * \Re(\underline{h_{z_j}})$

depend on the distance z_j to the hologram and on the object aperture ϑ_j (defined as the indicator function of the projection of the j-th object). They are implanted on points of a 2D Poisson point process resulting from the projection with intensity $c \cdot e$ (e being the thickness of the volume) and whose realization is the set of $(x_j, y_j)_j$ objects locations.

The reconstruction of the volume recorded in a hologram is based on the diffraction of a plane wave by the hologram. The digital processing of a hologram is traditionally carried out via convolution with Fresnel functions. An in-focus image of an object is obtained when the parameter of the Fresnel function $\underline{h_z}$ matches the object-hologram distance. This is made possible thanks to the inversion property of Fresnel function: $\underline{h_z} * \underline{h_{-z}} = \delta_{0,0}$. The physical interpretation of this property is the well-known principle of ray reversibility. The real part of Fresnel functions satisfies a weakened version: $\Re(\underline{h_z}) * \Re(\underline{h_{-z}}) = \frac{1}{2}[\delta_{0,0} + \Re(\underline{h_{2z}})]$. As Fresnel functions are symmetrical and $\Re(\underline{h_{-z}}) = \Re(\underline{h_z})$, the last equation can be rewritten in terms of cross-correlation: $\Re(\underline{h_z}) \star \Re(\underline{h_z}) = \frac{1}{2}[\delta_{0,0} + \Re(\underline{h_{2z}})]$ (with $\star$ denoting the cross-correlation operation, connected to the convolution through the relation $f \star g = f * \check{g}$ with f and g any distribution and $\check{g}$ the symmetric of g with respect to the origin). The aperture of object j is nearly recovered when the jth diffraction pattern $\vartheta_j * \Re(\underline{h_{z_j}}) * \delta_{x_j,y_j}$ is cross-correlated with $\Re(\underline{h_{z_j}})$. This is the basic principle classically used in digital in-line holography. The distance z_j has to be known in order to get an in-focus image of the object.

Instead of using $\Re(\underline{h_{z_j}})$ to perform the cross-correlation, the diffraction pattern can be autocorrelated. The (x_j, y_j) location is then lost and the remaining terms are: $\frac{1}{2}\vartheta_j \star \vartheta_j + \frac{1}{2}\vartheta_j \star \vartheta_j * \Re(\underline{h_{2z_j}})$. The autocorrelation of the centered hologram intensity $\tilde{I}_H$ (i.e. its autocovariance) can be expanded into three terms(Denis *et al.*, 2006):

$$\begin{aligned} \tilde{I}_H \star \tilde{I}_H \propto 2 \sum_{j=1}^{N} \vartheta_j \star \vartheta_j + 2 \sum_{j=1}^{N} \vartheta_j \star \vartheta_j * \Re(\underline{h_{2z_j}}) \\ + 4 \sum_{j=1}^{N} \sum_{\substack{k=1 \\ k \neq j}}^{N} \vartheta_j \star \vartheta_k * \Re(\underline{h_{z_j}}) * \Re(\underline{h_{z_k}}) * \delta_{x_j - x_k, y_j - y_k}. \end{aligned} \tag{4}$$

The first term corresponds to the mean geometrical covariogram of the apertures (up to a proportionality factor accounting for the number of objects and experimental parameters

such as the camera gain and the laser power); the second to a virtual image of the geometric covariogram; the third to slightly out-of-focus and largely out-of-focus cross-correlation terms. It has been shown in the quantitative study carried out in reference (Denis *et al.*, 2006) that the MGC dominates the other terms on most of its range. Thus, in the case of holograms of low-concentration volumes and under the assumption of a homogeneous Poissonian object process, the hologram autocovariance leads to a good estimate of the MGC.

4. Reconstruction of the rose of directions

We have shown in the previous section that the mean geometric-covariogram (MGC) can be estimated easily from a hologram. The MGC carries information about the direction, size and shape of the objects projections. However the contributions of shape(s) and size(s) mix with that of directions. The resulting MGC can therefore be difficult to interpret quantitatively. We describe in this section how the MGC can be processed to get a reconstruction of a rose of directions.

In the general case, only a projection of the rose of directions of the objects can be reached from the estimated MGC. We describe in section 4.A how the 2D rose of directions can be derived form the MGC. We then describe in section 4.B how the MGC of the objects projections can be connected with the theoretical geometric-covariogram of a parametrized model. The MGC can easily be computed for given shapes, sizes and directions of the objects. The reconstruction problem of the 3D rose of directions is an inverse problem. Due to the projection operation that connects the objects to the MGC, additional information is required to reconstruct the 3D rose of directions. We suggest a reconstruction algorithm in the case of short fibers under the assumption of constant and known object size. This description is of more general scope and the derivation can easily be carried out for other types of shapes.

4.A. Derivation and inversion of the rose of intercepts

We review in this paragraph the first possible approach for MGC processing: the derivation of the rose of intercepts.

The rose of intercepts $\gamma(\alpha)$ defines the diametral variation in the direction orthogonal

to α. It can be easily measured on an image of the objects. In our case, objects are not directly accessible and the rose of intercepts must be derived from the MGC expressed in polar coordinates $\bar{k}(r,\alpha)$ using the following relation (Serra, 1982):

$$\gamma(\alpha) = -\left.\frac{\partial \bar{k}(r,\alpha)}{\partial r}\right|_{r=0} \tag{5}$$

The rose of directions can then be reconstructed from the rose of intercepts using one of the inversion schemes described in the literature (see reference (Kiderlen & Pfrang, 2005) for an overview of available methods).

This approach is however limited by the difficulty to get a robust estimation of the zero derivative of the MGC as the presence of uncorrelated noise in the hologram tends to interfere with it. Furthermore, the MGC is underused which is regrettable as the underlying inverse problem is ill-posed. To circumvent these drawbacks, a more general approach making use of the whole MGC is described in the following paragraphs. The objects under study to illustrate the reasoning are micro-fibers.

4.B. Formulation of the general inverse problem

We derive in this section the connection between the MGC, estimated directly from the hologram, and the distribution of directions of the underlying fiber population.

Let a short fiber be defined by its direction (θ,ϕ) (given in spherical coordinates), its length L and its thickness t (see Figure 2). Its projection along the z axis can be approximated by a rectangle of height $h = t$ and width $w = L\sin\phi + t\cos\phi$.

The geometric covariogram $K(r,\alpha)$ of a $w \times h$ rectangle directed along θ is the common area between the rectangle and its translate by a vector of length r and direction α (see Figure 3):

$$\begin{cases} K_{t,L,\theta,\phi}(r,\alpha) = (w - r|\cos(\alpha-\theta)|)\,(h - r|\sin(\alpha-\theta)|) \\ \qquad\qquad \text{if} \quad w - r|\cos(\alpha-\theta)| \geq 0 \quad \text{and} \quad h - r|\sin(\alpha-\theta)| \geq 0; \\ K_{t,L,\theta,\phi}(r,\alpha) = 0 \text{ if not.} \end{cases} \tag{6}$$

A graphical representation of the geometric covariogram is given in Figure 4.

As the contribution of each fiber is added to form the mean geometric covariogram (see section 3), the overall MGC $\bar{k}$ is connected to the density $f(t, L, \theta, \phi)$ of sizes and directions through the integral relation:

$$\underbrace{\bar{k}(r,\alpha)}_{\text{data}} = \iiiint \underbrace{K_{t,L,\theta,\phi}(r,\alpha)}_{\text{model}} \underbrace{f(t,L,\theta,\phi)}_{\text{unknown}} \mathrm{d}t\mathrm{d}L\mathrm{d}\theta\mathrm{d}\phi + \underbrace{n(r,\alpha)}_{\text{noise}}. \tag{7}$$

This equation links together the data and the unknown and underlines the inverse problem nature of the reconstruction. The geometric covariogram $K_{t,L,\theta,\phi}(r,\alpha)$ represents the model of the shape/size/direction dependency in the MGC and is known analytically. Since the MGC is obtained from experimental data and with an approximation, we introduce a noise term that represents the difference between the modelization and the actual data.

Equation 7 expresses both a projection operation and an integration over all possible objects. The reconstruction of the density f requires to invert both operations. The projection can not be inverted without prior information. Therefore, the scheme to recover the 3D density information described in the following subsections rely on necessary assumptions.

4.C. Discrete problem

We describe here how equation 7 can be sampled and we suggest an iterative algorithm to reconstruct the unknown distribution f under additional assumptions.

The number of parameters must first be reduced in order to allow the reconstruction. Two problems of interest can be studied:

(P1) reconstruct the 3D direction distribution under the assumption that t and L are known and constant;

(P2) reconstruct the 2D direction and projected length distribution of fibers under the assumption that t is known and constant (only the projection of the directions is studied).

These two problems are of equivalent difficulty since the projected length and the out-of-plane direction play similar roles in the expression of the geometric covariogram K. We

therefore describe the reconstruction of $f(\theta, \phi)$ in the case of fibers of constant length. The results obtained can directly be adapted to problem **P2**.

The MGC is estimated on a disc that includes the bounded support of the MGC. The sampling used is Cartesian as the estimation is based on Fourier transforms. The noise $n(r, \alpha)$ associated with the data is not stationary as it is derived from an autocorrelation. To take into account the difference in noise level between the center of the autocorrelation and farther regions, we introduce a weighting matrix W that reduces the influence of data points with low confidence due to the noise level. W is defined in the general case as the inverse data-covariance matrix $W = cov(\bar{k})^{-1}$.

The unknown distribution f is computed at chosen points (θ, ϕ). To compare easily the reconstructed density in two different directions one has to use a uniform sampling in θ. A uniform sampling in spherical coordinates would lead to an over-sampling effect for directions close to $\phi = 0$. This region however is badly defined as the directions are nearly collinear to the projection direction. A form of regularization can be introduced by using a looser sampling than spherical coordinates. Since the direction discrimination is connected with the difference between the projections, the sampling can be defined uniformly in the projected space (i.e. in a disc). For this purpose, we chose a sampling based on a spiral distribution inspired from the paper (Rakhmanov *et al.*, 1994).

The discretized form of equation 7 can be written as a matrix product:

$$\begin{array}{ccccccccc}
\begin{bmatrix} \bar{k}(r_1, \alpha_1) \\ \vdots \\ \bar{k}(r_n, \alpha_1) \\ \vdots \\ \bar{k}(r_n, \alpha_m) \end{bmatrix} & = & \begin{bmatrix} K_{\theta_1,\phi_1}(r_1, \alpha_1) & \cdots & K_{\theta_p,\phi_q}(r_1, \alpha_1) \\ \vdots & & \vdots \\ K_{\theta_1,\phi_1}(r_n, \alpha_1) & \cdots & K_{\theta_p,\phi_q}(r_n, \alpha_1) \\ \vdots & & \vdots \\ K_{\theta_1,\phi_1}(r_n, \alpha_m) & \cdots & K_{\theta_p,\phi_q}(r_n, \alpha_m) \end{bmatrix} & \begin{bmatrix} f(\theta_1, \phi_1) \\ \vdots \\ f(\theta_p, \phi_1) \\ \vdots \\ f(\theta_p, \phi_q) \end{bmatrix} & + & \begin{bmatrix} n(r_1, \alpha_1) \\ \vdots \\ n(r_n, \alpha_1) \\ \vdots \\ n(r_n, \alpha_m) \end{bmatrix} \\
\bar{\mathbf{k}} & = & \mathbf{K} & \mathbf{f} & + & \mathbf{n}
\end{array}, \tag{8}$$

where (r_k, α_l) represents a sampling point in the autocorrelation space, (θ_k, ϕ_l) a sampling point in the directions space $(\mathcal{S}^2)$ and bold faced symbols $\bar{\mathbf{k}}$, $\mathbf{K}$, $\mathbf{f}$ and $\mathbf{n}$ are compact notations

for their vector and matrix counterparts.

4.D. Reconstruction algorithm

There exists a wide range of reconstruction algorithms to solve inverse problems. The choice of a specific approach requires to analyze the characteristics of the problem and especially to identify general properties common to all possible solutions: *a priori* knowledge. In the case of the rose of directions of fibers, a reconstruction of the rose is of special interest only if there exists one or a few significant directions. The distribution of directions f then is close to zero for all directions but that of the fibers. This "mainly zero" characteristic together with the positivity constraint ($f(\theta,\phi) \geq 0$ for all (θ,ϕ)) lead us to use a constrained maximum likelihood approach: the solution $f^{(\mathrm{ML})}$ is that which maximizes the likelihood under the positivity constraint:

$$f^{(\mathrm{ML})} = \arg\max_f \Pr(\bar{k}|f) = \arg\max_f \phi_{\mathrm{ML}}(f), \text{ subject to } \forall\,(\theta,\phi), f(\theta,\phi) \geq 0, \tag{9}$$

with $\phi_{\mathrm{ML}}(f)$ the log-likelihood: $\phi_{\mathrm{ML}}(f) \propto \log[\Pr(\bar{k}|f)]$+constant.

Well known and easy to implement iterative algorithms have been proposed to solve such problems. They are referred to as multiplicative algorithms (Lantéri *et al.*, 2002) and differ depending on the noise nature. In the case of Poissonian noise, two identical algorithms have been introduced: Richardson-Lucy Algorithm (Richardson, 1972; Lucy, 1974) and the expectation-maximization procedure (Shepp & Vardi, 1982). In the case of Gaussian noise, the Image Space Reconstruction Algorithm (ISRA) builds a solution through the following recursion formula (Daube-Witherspoon & Muehllehner, 1986):

$$\mathbf{f}_j^{(k+1)} = \mathbf{f}_j^{(k)} \frac{\left(\mathbf{K}^{\mathrm{T}}\mathbf{W}\bar{\mathbf{k}}\right)_j}{\left(\mathbf{K}^{\mathrm{T}}\mathbf{W}\mathbf{K}\mathbf{f}^{(k)}\right)_j}, \tag{10}$$

where the subscript $\cdot_j$ denotes element j of the vector, and the superscript $\cdot^{\mathrm{T}}$ is used for the transpose operator. As long as the initial value $\mathbf{f}^{(0)}$ is positive, the reconstructed densities $\mathbf{f}^{(k)}$ remain positive (or null) as the iterative definition of equation 10 involves only positive reals. Let us notice that the mean geometric covariogram is known up to a proportionality factor,

$\mathbf{f}$ is therefore retrieved up to that factor and the actual density is obtained by normalization by $\sum_j \mathbf{f}_j$.

$\mathbf{W}$ clearly appears as a weighting factor that reduces the influence of data values with high noise variance. Even if the Gaussian model does not in our case appear as a natural model, this weighting capability (i.e. non-stationarity) is of great interest and overcomes the validity considerations on the Gaussian hypothesis. The approximations described in section 3 indeed lead to a bias that depends on (r, α) parameters. To take into account this bias, one can weight the data to give less influence to data points subject to higher bias.

5. Application to holograms of paper fibers

The model of short fibers introduced in the previous section can be applied to different kind of objects. The main constraint is that the fibers are required to be straight which is often true for short enough fibers (less than a millimeter). We worked on paper fibers as the on-line study of fiber directions in the very first step of paper making can have significant impact for paper industry.

The principles presented in section 4 are illustrated here on simulated and experimental data. The scheme of the proposed method to reconstruct a distribution of 3D directions in the case of fibers of constant size is depicted on Figure 5. A hologram is processed in two steps: first, the MGC is estimated as described in section 3; then the MGC is inverted to reconstruct the distribution of directions, based on section 4. Results are given on simulated data in the following subsection. In the case of fibers with variable lengths, the derivation of the rose of intercepts is illustrated on an experimental hologram in section 5.B.

5.A. Numerical simulation

The diffraction approximation (equation 1) makes it possible to simulate holograms. Our method can then be confirmed and the precision of the reconstruction assessed by comparing the retrieved distribution with the underlying exact distribution of the random process used to generate numerically the hologram.

Fiber population A set of 100 fibers was generated according to a random uniform distribution in a $7mm \times 7mm \times 7mm$ volume (fig. 6). The fibers are oriented along one of two mean directions: $(\theta_1, \phi_1) = (57°, 30°)$ and $(\theta_2, \phi_2) = (18°, 83°)$. Two thirds of the fibers have a direction close to (θ_1, ϕ_1), with a standard deviation of 4°; the last third is directed following to (θ_2, ϕ_2) with a lower standard deviation (1.5°). The fibers are $20\mu m$ thick and $500\mu m$ long.

Figure 6(a) displays a 3D view of the fibers. The distribution of directions is shown on Fig. 6(b): directions are represented as vertices on a discretization of the unit sphere.

Simulated hologram A hologram of the fibers is simulated according to equation 1. The distance between the volume of fibers and the hologram is set to 100mm along the z axis (see fig. 6(a)). The resulting 1024×1024 hologram with $6.7\mu m$ pixel width is displayed in Figure 7. We use it as the input of our algorithm to reconstruct the direction distribution.

MGC estimation The first step consists in estimating the MGC. We have shown that the hologram autocovariance is related to the MGC of the fibers projections. Figure 8(a) illustrates the autocovariance of the simulated hologram. Unwanted oscillations can be noticed outside of the MGC domain. The autocovariance therefore is thresholded to determine a domain of confidence. Figure 8(b) displays the autocovariance over this domain. The data restricted to the domain of confidence is not sufficient to guarantee fast convergence of the inversion algorithm in the next step. Data is therefore extrapolated outside the domain in polar coordinates (1D interpolation) to determine the domain where the MGC is null (Figure 8(c)). Data extrapolated (i.e. outside of the domain of confidence and non null) is not used in the inversion step; only the domain where the MGC is null is kept to reinforce the inversion constraints.

Reconstruction of the distribution of 3D directions The MGC can then be inverted using equation 10. Figure 9 displays the reconstructed distribution after a thousand iterations. A comparison of the retrieved distribution with the exact distribution (Figure

6(b)) shows good agreement. The whole reconstruction process takes about 30 seconds using Matlab® language on a Pentium 4 3GHz PC. The convergence speed can be improved by using a C language implementation in combination with techniques such as the non-linear conjugate gradients or the limited-memory variable metric methods described in (Thiébaut, 2002).

5.B. Experimental hologram of fibers

We illustrate the general case of fibers with varying sizes and directions in this paragraph.

Objects The objects under study are short paper fibers spread on a glass plate with a brush. The choice of a planar distribution of the fibers was caused by the ease to depict the actual distribution. A reconstructed plane can be computed to show an image of the fibers, for pedagogical reasons.

Hologram The hologram is recorded at $50mm$ from the glass plate with a $632nm$ HeNe laser. The camera used has a 1024×1280 pixel array with $6.7\mu m$ pixel width. The hologram is displayed on Figure 10.

Estimated rose of intercepts The MGC is estimated from the hologram using the autocovariance technique described in section 3. The derivative at the origin of the MGC is then estimated using a mean square approach (Serra, 1982) to get the rose of intercepts as pointed out in paragraph 4.A. The resulting rose of intercepts is shown on Figure 11. Its shape is characteristic of an anisotropic image. This can be confirmed with the reconstructed image computed in Figure 12.

The 2D rose of directions of the fibers projections can be computed by inverting the rose of intercepts (see section 4).

6. Conclusion

We have described and illustrated in this paper an original stereological approach for in-line digital holograms. The use of an imaging technique capable of fast 3D acquisition in association with direct processing of the data leads to a system suitable for on-line control.

In-line digital holography gives access to moving objects in a deep field (edges a few centimeters long). The hologram can be approximated as a sum of diffraction patterns corresponding to each object. The hologram auto-covariance then appears to lead to a good estimate of the MGC of the projections of the objects. The MGC carries interesting information on the shape of the projection of the objects. In the case of anisotropic objects such as fibers, the MGC can be used to estimate the main direction of a set of objects, as classically done with conventional images. Our MGC derivation from a hologram extends this method to "diffractive projections" of the objects.

In order to get quantitative results, the MGC requires further processing. The reconstruction of the distribution of directions of the objects is an inverse problem that requires additional knowledge to be inverted. We have suggested a scheme to reconstruct the 3D rose of directions of fibers under the assumption of known and unique size. If no assumption can be done on the fibers sizes or directions, only the 2D rose of the projected directions can be derived through the computation of the rose of intersection from the MGC.

We illustrated both cases on simulated or real data. We focused our attention on the extraction of the direction information rather than on an exhaustive study of the performance of our inversion technique. Good results are obtained with our inversion method when there are only a few main directions. Further work should focus on both the robustness of the inversion algorithm and on further improving its convergence speed.

Acknowledgements

This research was supported by a grant from Rhône-Alpes region.

References

Daube-Witherspoon, M. E. & Muehllehner, G. (1986). An iterative image space reconstruction algorithm suitable for volume ECT. *IEEE Trans. Med. Imaging*, **5**, 61–66.

Denis, L., Fournier, C., Fournel, T., Ducottet, C. & Jeulin, D. (2006). Direct extraction of mean particle size from a digital hologram. *Applied Optics*, **45**, 944–952.

Goodman, J. (1996). *Introduction to Fourier Optics*. Mc Graw-Hill.

Jeulin, D. (1992). Multivariate random image models. In *8th ISS Congress*, vol. 11/SUPPL I, 59–66. Acta Stereologica, Irvine, CA.

Kiderlen, M. & Pfrang, A. (2005). Algorithms to estimate the rose of directions of a spatial fibre system. *J. Microsc.*, **219**, 50–60.

Lantéri, H., Roche, M. & Aime, C. (2002). Penalized maximum likelihood image restoration with positivity constraints: multiplicative algorithms. *Inverse Problems*, **18**, 1397–1419.

Lucy, L. B. (1974). An iterative technique for the rectification of observed distributions. *Astron. J.*, **79**, 745–754.

Onural, L. (1993). Diffraction from a wavelet point of view. *Optics Letters*, **18**, 846.

Poon, T.-C., Yatagai, T. & Jüptner, W., eds. (2006). *Special Issue: Digital Holography*, vol. 45 of *Applied Optics*.

Rakhmanov, E. A., Saff, E. B. & Zhou, Y. M. (1994). Minimal discrete energy on the sphere. *Mathematical Research Letters*, **1**, 647–662.

Richardson, W. H. (1972). Bayesian-based iterative method of image restoration. *J. Opt. Soc. Am.*, **62**, 55–59.

Royer, H. (1974). An application of high-speed microholography: the metrology of fogs. *Nouv. Rev. Opt*, **5**, 87–93.

Serra, J. (1968). Les fonctions aléatoires de dilution. Tech. Rep. 37, CMM, Paris School of Mines publication.

Serra, J. (1982). *Image Analysis and Mathematical Morphology*. Academic, New York.

Shepp, L. A. & Vardi, Y. (1982). Maximum likelihood reconstruction for emission tomography. *IEEE Trans. Med. Imaging*, **1**, 113–122.

Stoyan, D. & Beneš, V. (1991). Anisotropy analysis for particle systems. *J. Microsc.*, **164**, 159–168.

Thiébaut, E. (2002). Optimization issues in blind deconvolution algorithms. In *Astronomical Data Analysis II*, edited by J.-L. Starck & F. D. Murtagh, vol. 4847, 174–183. SPIE.

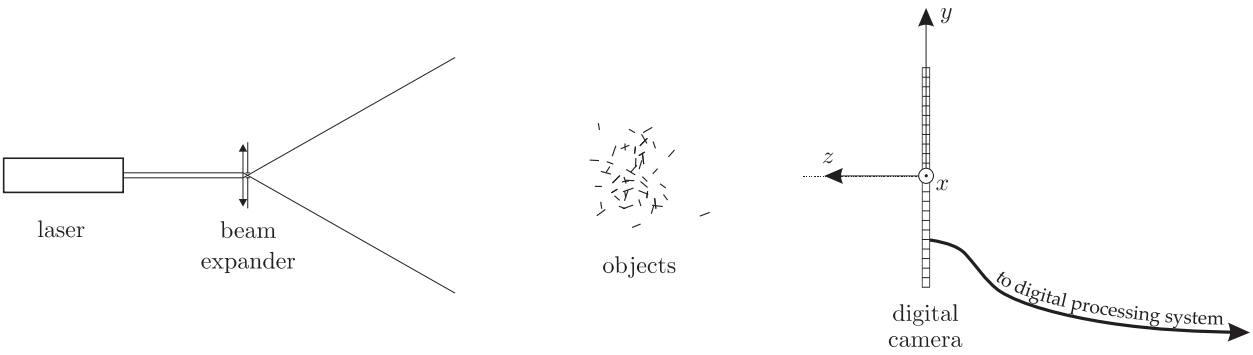

Fig. 1. Optical setup used in digital in-line holography

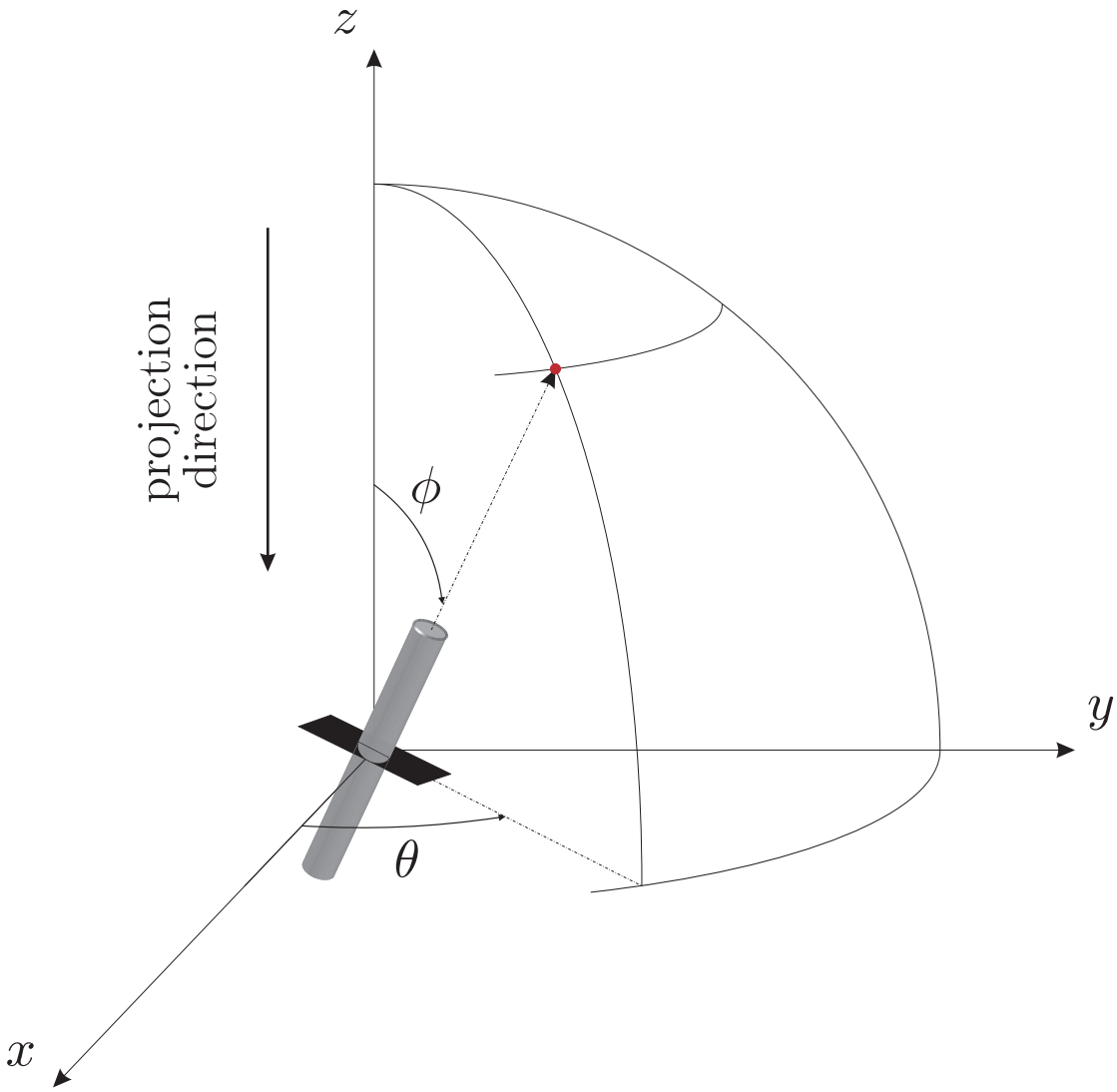

Fig. 2. Model of a short fiber and its orthogonal projection along the optical axis

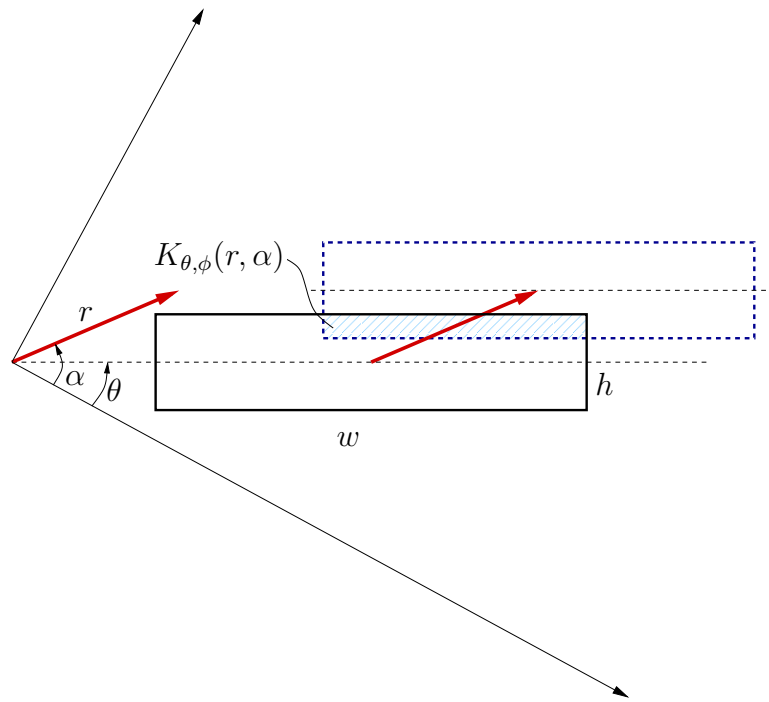

Fig. 3. Geometric covariogram $K(r, \alpha)$ of a rectangle (hatched area)

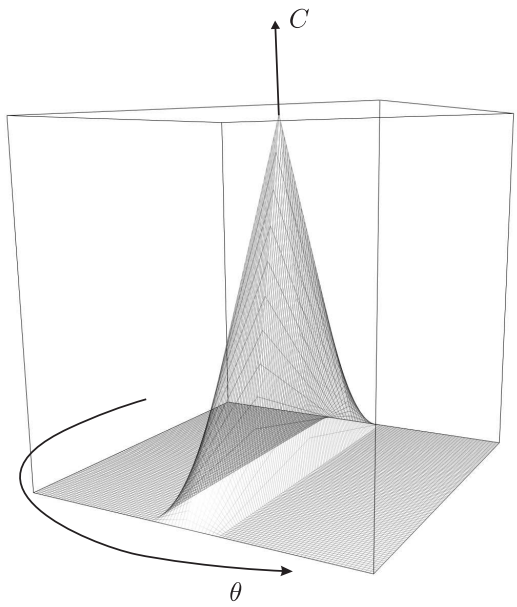

Fig. 4. Geometric covariogram of a rectangle with $w = 5h$

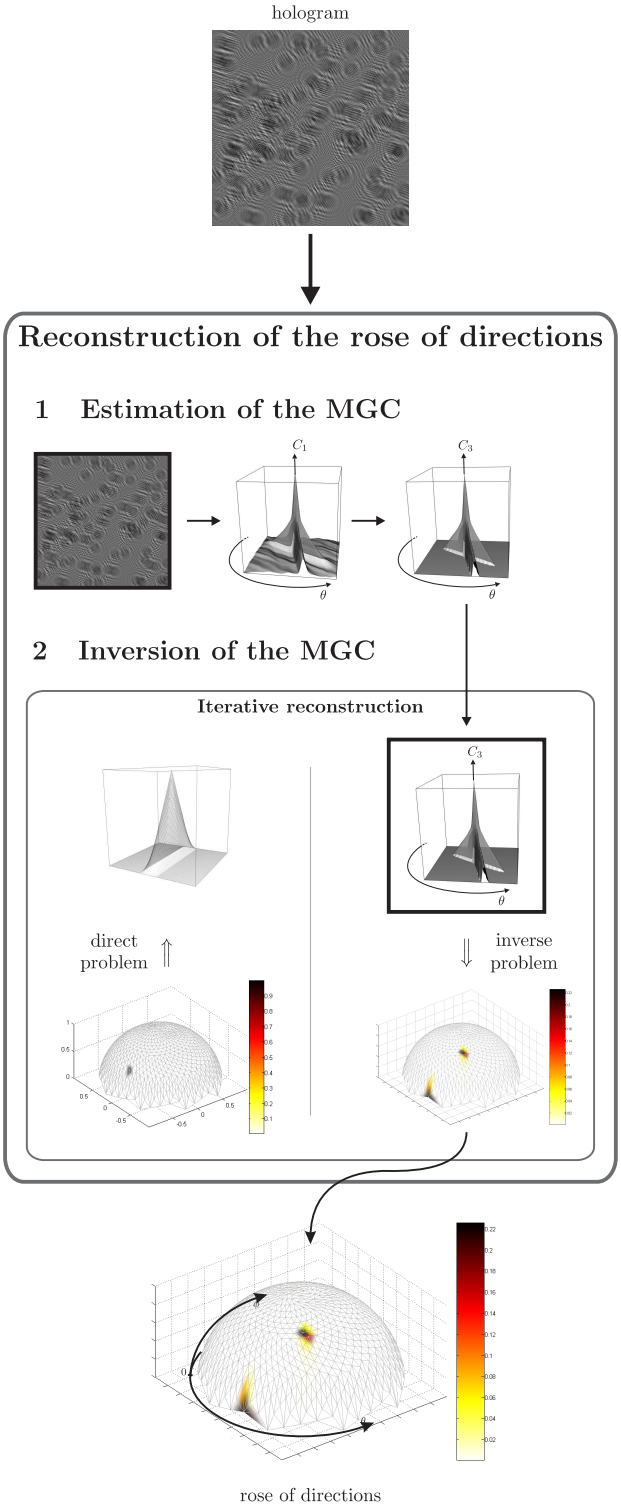

Fig. 5. Scheme of the method to reconstruct the rose of directions from an in-line hologram

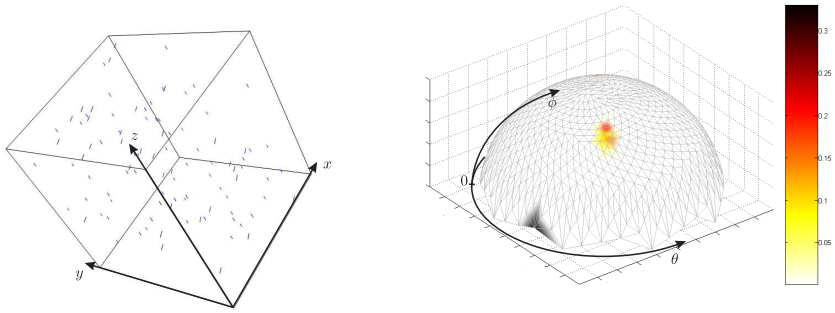

(a) (b)

Fig. 6. Fiber population used in the numerical simulation: (a) 3D view of the studied volume; (b) corresponding distribution of fiber directions

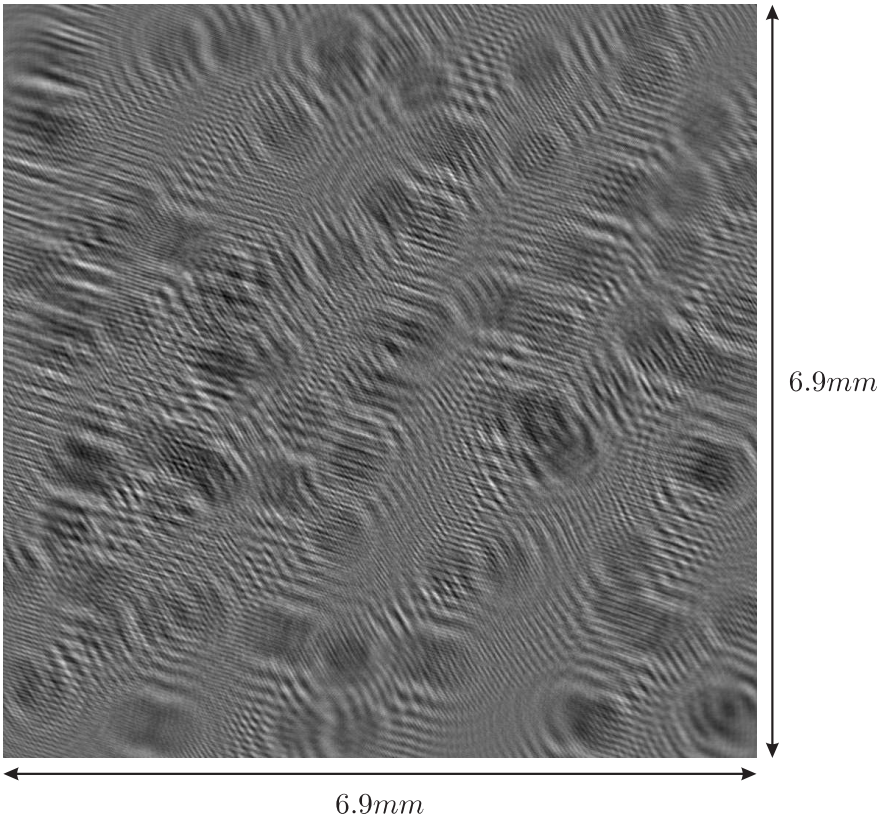

Fig. 7. Simulated hologram of the volume of fibers displayed in Figure 6

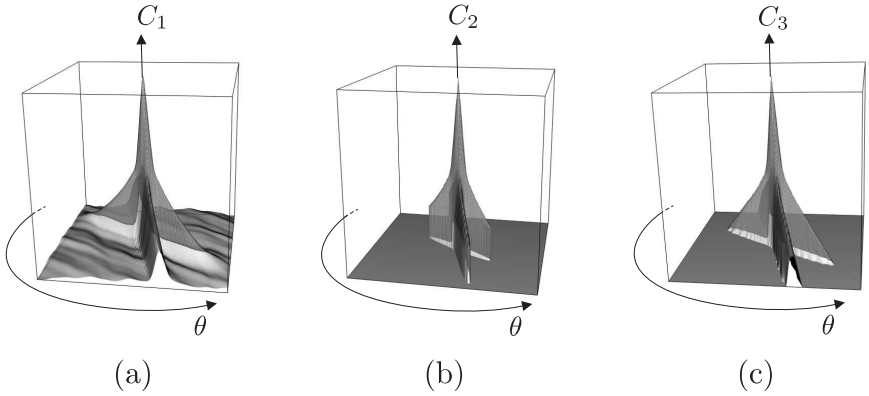

Fig. 8. MGC estimation: (a) hologram auto-covariance; (b) auto-covariance restricted to the domain of confidence; (c) MGC estimation: linear radial extrapolation of (b)

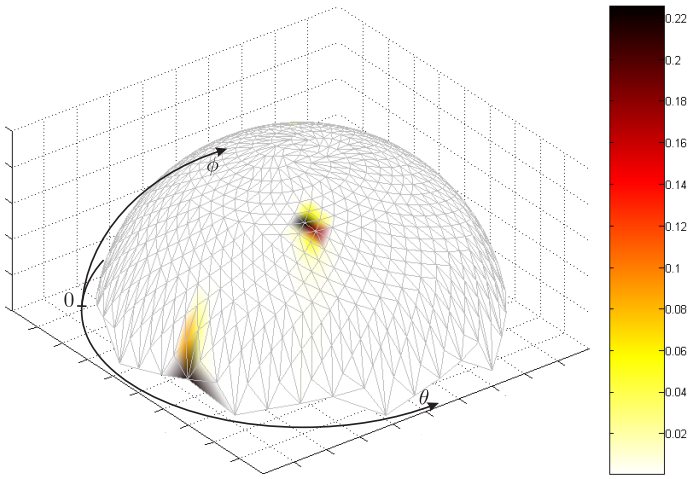

Fig. 9. Retrieved distribution of directions from the simulated hologram of Figure 7 through MGC inversion.

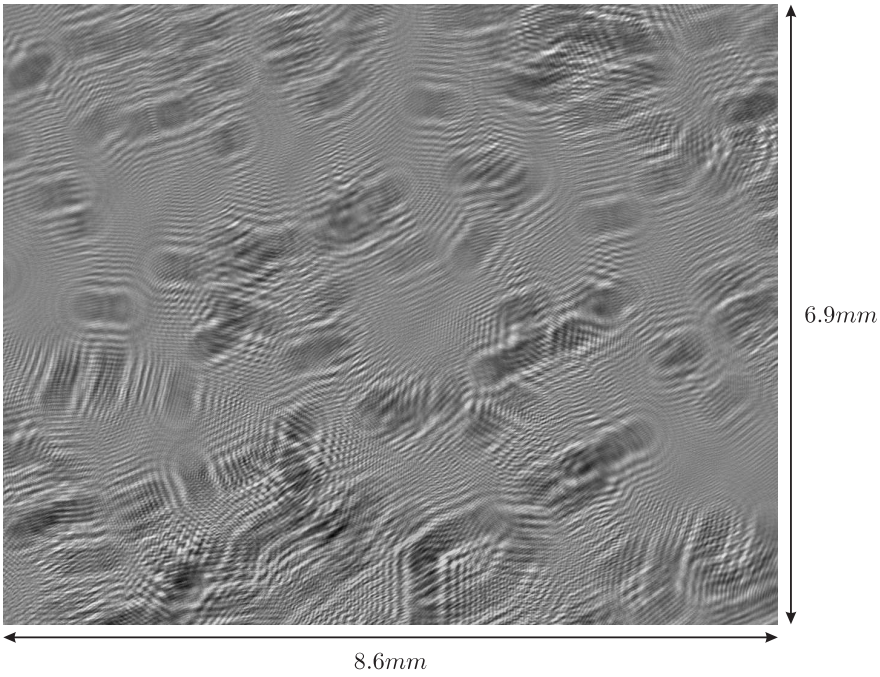

Fig. 10. Experimental hologram of paper fibers spread on a glass plate.

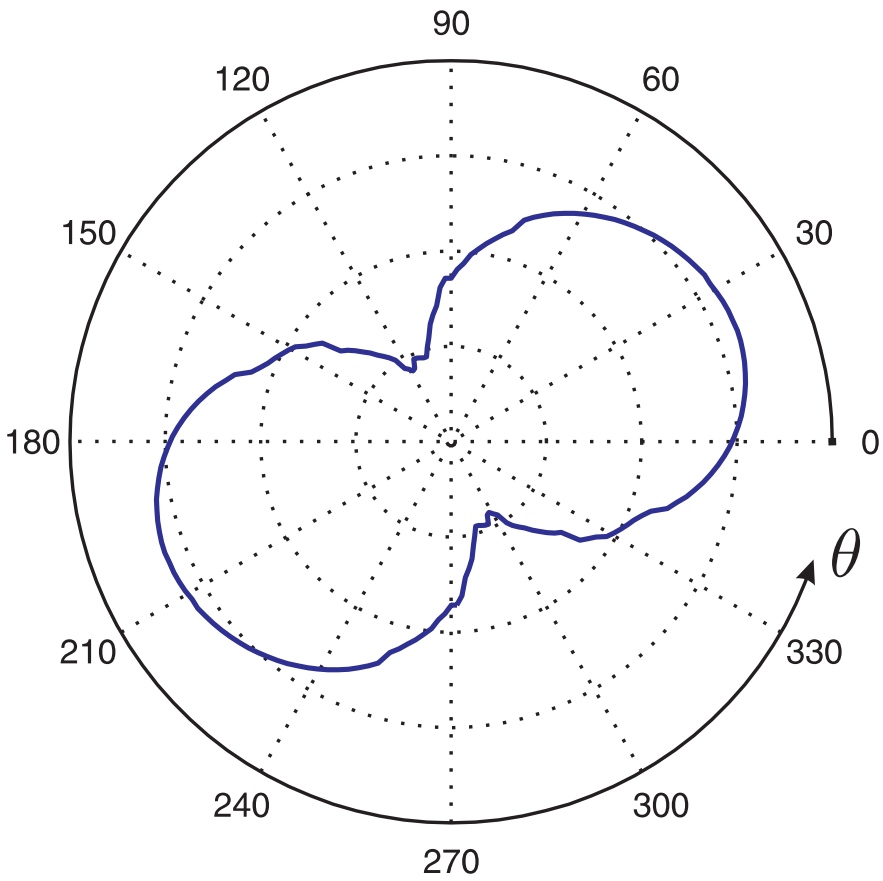

Fig. 11. Rose of intercepts derived from the MGC estimated from hologram of Figure 10.

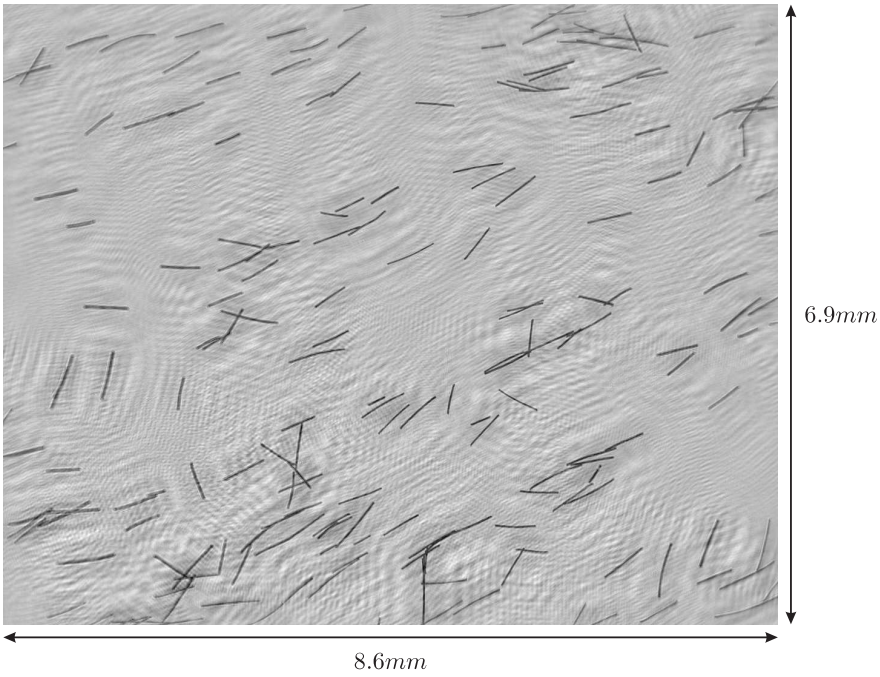

Fig. 12. Reconstructed plane of the fibers showing their varying sizes and directions.